

Designing cooperatively folded abiotic uni- and multimolecular helix bundles

Soumen De, Bo Chi[†], Thierry Granier, Ting Qi[†], Victor Maurizot and Ivan Huc^{*}

Abiotic foldamers, that is foldamers that have backbones chemically remote from peptidic and nucleotidic skeletons, may give access to shapes and functions different to those of peptides and nucleotides. However, design methodologies towards abiotic tertiary and quaternary structures are yet to be developed. Here we report rationally designed interactional patterns to guide the folding and assembly of abiotic helix bundles. Computational design facilitated the introduction of hydrogen-bonding functionalities at defined locations on the aromatic amide backbones that promote cooperative folding into helix–turn–helix motifs in organic solvents. The hydrogen-bond-directed aggregation of helices not linked by a turn unit produced several thermodynamically and kinetically stable homochiral dimeric and trimeric bundles with structures that are distinct from the designed helix–turn–helix. Relative helix orientation within the bundles may be changed from parallel to tilted on subtle solvent variations. Altogether, these results prefigure the richness and uniqueness of abiotic tertiary structure behaviour.

In the past 20 years, chemists have shown that numerous non-natural foldamer backbones adopt well-defined conformations analogous to the secondary motifs of biopolymers, such as helices, sheets and turns^{1–5}. This new paradigm holds great promise for molecular design. Indeed, biopolymers' efficient and sophisticated functions in terms of recognition, catalysis, information storage and transfer, or energy conversion, rest on their specific shapes obtained through folding of their primary sequence. Folding emerges as the most-efficient strategy to organize large and complex arrays of chemical groups in space with atomic precision. In addition, molecules that consist of a linear sequence of building blocks possess the advantage of being inherently modular and amenable to optimization through iterative modifications, for example, mutations and deletions or additions of monomers or longer segments. In this context, abiotic foldamers that have backbones chemically remote from the natural peptidic and nucleotidic skeletons are particularly interesting because they may give access to shapes, and thus to functions, different to those of peptides and nucleotides, just like the shapes and functions of peptides and nucleotides differ from each other because of their distinct chemical compositions. For example, foldamers that have aromatic moieties in their main chain constitute a distinct grouping that has been shown to form unusual structures, such as pillars⁶, knots^{7,8} or helices of variable diameter^{9,10}.

However, most of the functions of biopolymers, especially of proteins, emerge at the level of their tertiary structures and would not be achieved by an isolated α -helix or β -sheet. A major challenge thus resides in establishing design principles of artificial tertiary folds that comprise several secondary structural elements. The highly cooperative nature of the tertiary folds means that the protein design itself remains a very challenging endeavour despite great advances^{11–14}, which include the development of dedicated computational tools¹⁵. Changing an α -amino acid sequence to optimize interactions between secondary motifs may also alter interactions within them and thus decrease the overall conformational stability. Nevertheless, α -helix bundling is a specific pattern that

can largely be predicted, which allows the design of self-assembled quaternary bundles^{12,16–19} as well as of novel tertiary structures²⁰. Yet, the exploitation of non-natural monomers in artificial tertiary folds is limited. Several β -amino acids may be tolerated in known peptidic bundles or tertiary structures^{21–24}. Sheets that contain non-natural units have been reported as well^{25,26}. As key milestones, self-assembled helix bundles of β -peptides^{27,28} and of β -ureas²⁹ have been reported. Stitching helices together within these bundles may, in principle, yield an artificial tertiary fold, but this remains to be implemented. To the best of our knowledge, no genuine tertiary structures are known that do not contain α -amino acids. Examples that approach this simply connect several abiotic helices through short or rigid linkers^{30–32}, or non-covalently thread them onto rod-like templates³³. Going beyond the world of peptides, tertiary folds based on abiotic backbones remain an unexplored area. Given current standards in the fabrication of long sequences through solid-phase synthesis and ligation methods^{34–36}, synthesis itself may not constitute a major stumbling block towards artificial tertiary structures. It then appears that, even though interactions within abiotic secondary structural motifs are well understood and often predictable, interactions between secondary elements have escaped our prediction capabilities. Furthermore, until now tertiary folding and helix bundling have been limited to water.

In the following, we report our success at the rational design of helix–helix interactional patterns to form tertiary folds within abiotic aromatic amide sequences and the subsequent characterization of different quaternary folds based on the same patterns. The approach rests on rather simple structure-based considerations and computational tools. We exploited the high stability of aromatic amide helices^{37,38} that made a hierarchical approach to tertiary structure design possible: helices may not unfold on interacting with each other and may thus be used as stable construction modules. Nevertheless, we observed the typical cooperative behaviour associated with the simultaneous occurrence of a large number of interactions. We also demonstrate that tertiary

CBMN Laboratory, Université de Bordeaux, CNRS, IPB, Institut Européen de Chimie et Biologie, 2 rue Escarpit, 33600 Pessac, France. [†]Present addresses: State Key Laboratory of Materials-Oriented Chemical Engineering, Nanjing Tech University, No. 30 South Puzi Road, Pukou District, Nanjing 211816, China (B.C.); School of Chemistry and Chemical Engineering, University of Chinese Academy of Sciences, Beijing 100049, China (T.Q.). *e-mail: i.huc@iecb.u-bordeaux.fr

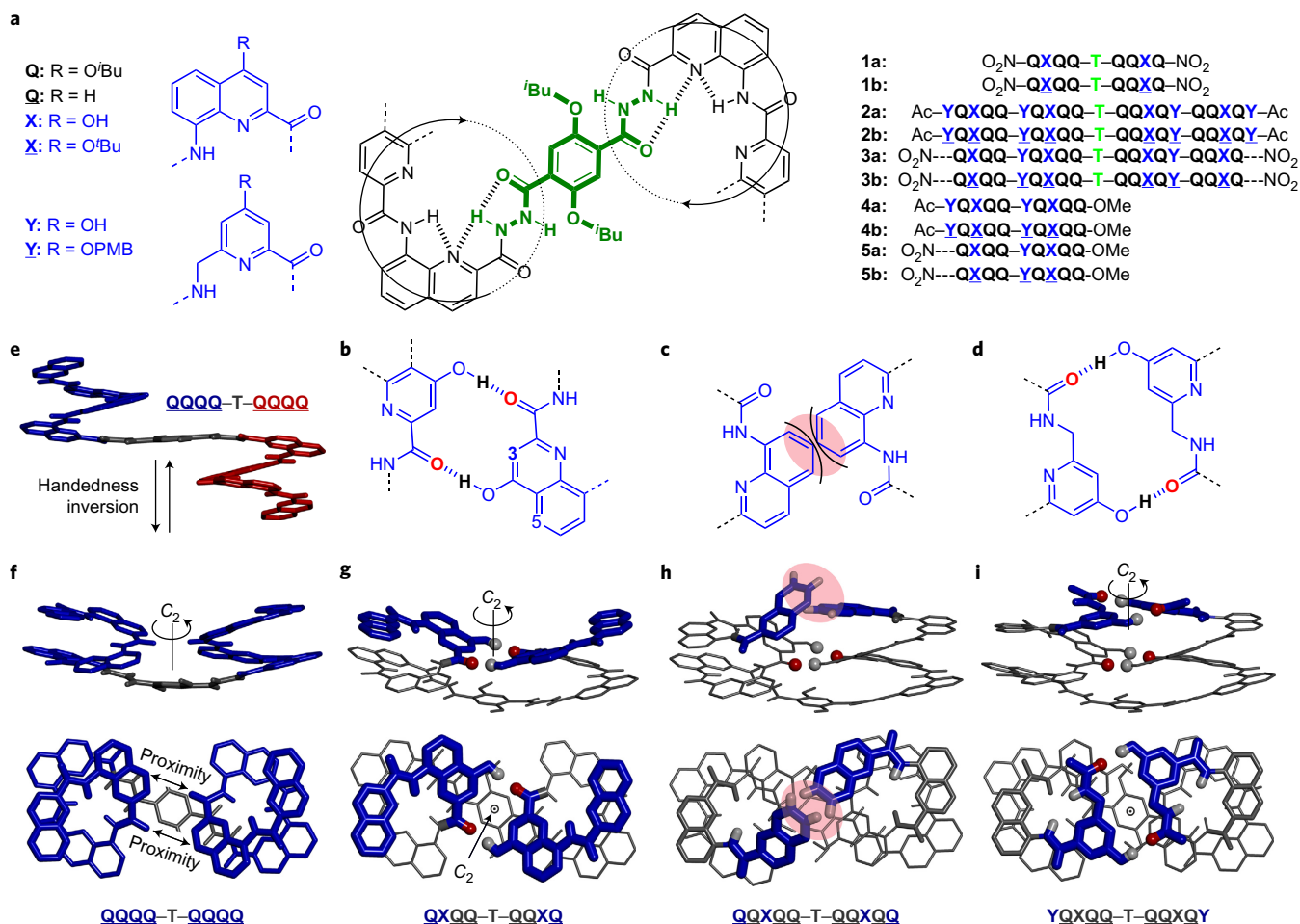


Figure 1 | Foldamer sequences and helix-turn-helix design. **a**, Structures of units **Q**, **X**, **Y** and **T** (green part only), and alignment of sequences 1-5. **X** and **Y** are the protected precursors of **X** and **Y**, respectively (PMB, 4-methoxybenzyl). **Q** lacks any side chain and was used in modelling studies only. Sequences are labelled 'a' when deprotected and 'b' when protected. The **T** units constitute an inversion of C→N sequence polarity; sequences that contain **T** thus have two N termini. Two circles schematize the projection of adjacent **Q_n** helices (in black) in the plane of **T** (in green). The arrows indicate in-plane clockwise rotation when going from the C to the N terminus of a **Q_n** helix. The actual helix handedness depends on whether the helix is above or below the plane. For sequences terminated with 8-nitro groups, this group is noted in the replacement of the NH group of **Q** or **X** units. **b-d**, Hydrogen bonds or steric hindrance critical in the models shown in **g-i**, respectively. **e-i**, Energy-minimized models. In **e** and **f**, the *P* and *M* helices are shown in blue and red, respectively. In **g-i**, the units of interest at the top of the structures are shown as thick blue tubes. In the models, the isobutoxy groups of **T** were replaced by methoxy groups. Protons and oxygen atoms involved in hydrogen bonds are shown as white and red balls, respectively. A pink surface indicates a steric clash in **c** and **h**.

folding may occur in apolar solvents and be driven exclusively by hydrogen bonds. These results show that rational design is a viable approach to artificial tertiary structures and pave the way to engineering more-complex and larger molecular shapes with atomic precision. Although function was not considered in the context of this study, abiotic tertiary folded objects prefigure the implementation of sophisticated molecular machineries, which include controlled motion, recognition and catalysis in media other than water.

Results and discussion

Design of tertiary structures. Oligoamides of 8-amino-2-quinoline-carboxylic acid **Q** (Fig. 1a) have been shown to adopt helical conformations stabilized by hydrogen bonds and electrostatic repulsions between quinoline nitrogen atoms and adjacent amide NH and CO groups, respectively, as well as by solvophobic forces associated with aromatic stacking^{2,37,39}. Non-covalent interactions within these helices thus generate well-understood motifs in which, unlike in peptides, the amide NH point towards and the amide CO point away from the helix axis. However, at the start of this work, there was no clue as to how to orchestrate interactions

between two helices and generate more-complex architectures. We set out to design a tertiary helix-turn-helix structure *ab initio* by simply examining computer models. We eventually found that a terephthalic acid bis-hydrazide **T** had an appropriate length to constitute a turn unit to link two helical **Q_n** segments. **T** inserts itself in the network of hydrogen bonds and prevents steric clashes between short helices while preserving enough proximity to be compatible with helix-helix interactions. Sequences such as **Q₄-T-Q₄**, in which quinoline rings are deprived of side chains, may thus adopt two conformations: a C₂ symmetrical conformer in which both **Q₄** helices have right-handed (*P*) helicity (or left-handed (*M*) helicity) and are on the same side of the turn; and a centrosymmetrical *PM* conformation in which helices are on opposite sides of the turn (Fig. 1e,f)⁴⁰. In the absence of helix-helix interactions, the *PP/MM* and *PM* conformers are expected to be equiprobable. A notable feature of the *PP/MM* conformer of **Q₄-T-Q₄** is the relative proximity (3.5–4 Å) between the carbonyl amide of the second quinoline of each **Q₄** segment (counting starts from the N terminus), and positions 3 and 4 of the second quinoline ring of the other **Q₄** segment (Fig. 1f). Based on this proximity, we inferred that a

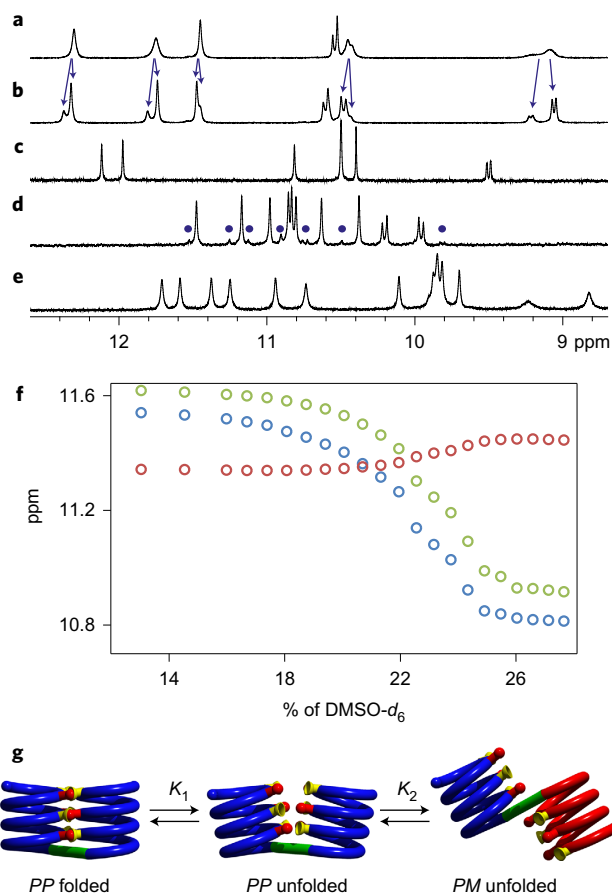


Figure 2 | Solution studies of helix-turn-helix motifs. a–e, Extracts of ¹H NMR spectra in CDCl₃ of **1b** at 25 °C (a), **1b** at 0 °C (b), **1a** at 25 °C (c), **2b** at 25 °C (d) and **2a** at 25 °C (e). Arrows and circles indicate the presence of a minor and major species assigned to PP/MM and PM conformers, respectively. f, Variations of the chemical shift of selected ¹H NMR signals of **2a** on the addition of DMSO-d₆ (Supplementary Fig. 12). g, Schematic representation of the equilibria involved in polar-solvent-induced helix-turn-helix unfolding. A similar equilibrium exists with the MM conformer.

hydrogen-bond donor at these positions might reach the carbonyl group and generate attractive interactions between the two helices. The 4-hydroxy group of unit X was thus added and energy-minimized models predicted the formation of inter-helix hydrogen bonds that stabilize the start of a helix-turn-helix motif in the PP/MM conformer (Fig. 1b,g).

This initial prediction was verified by experiments. Sequence **1b** was prepared (the synthetic schemes are given in Supplementary Figs 1–4). Its ¹H NMR spectrum in CDCl₃ at 25 °C shows slightly broadened resonances that split on cooling, consistent with the coexistence of PP/MM and PM conformers (Fig. 2a,b)³¹. One species is favoured, which we assume to be PM (see below). On the contrary, the deprotected sequence **1a** shows one set of sharp NMR signals (Fig. 2c). Diastereotopic motifs of the signals of ^tBuO side chains indicate a slow helix-handedness inversion on the NMR timescale, even at 25 °C (Supplementary Fig. 5), which implies that only one conformer could be detected. A crystal structure of **1a** was obtained (Fig. 3a) and shows a PP/MM helix-turn-helix essentially superimposable on the computer prediction.

Models of elongated sequences showed that an additional Q monomer leads to steric clashes between the helices: CH groups in positions 6 and 7 of the most peripheral quinoline rings hinder each other (Fig. 1c,h). Instead, monomer Y (Fig. 1a) brings the same contribution to helix curvature as X and yet lacks the aryl

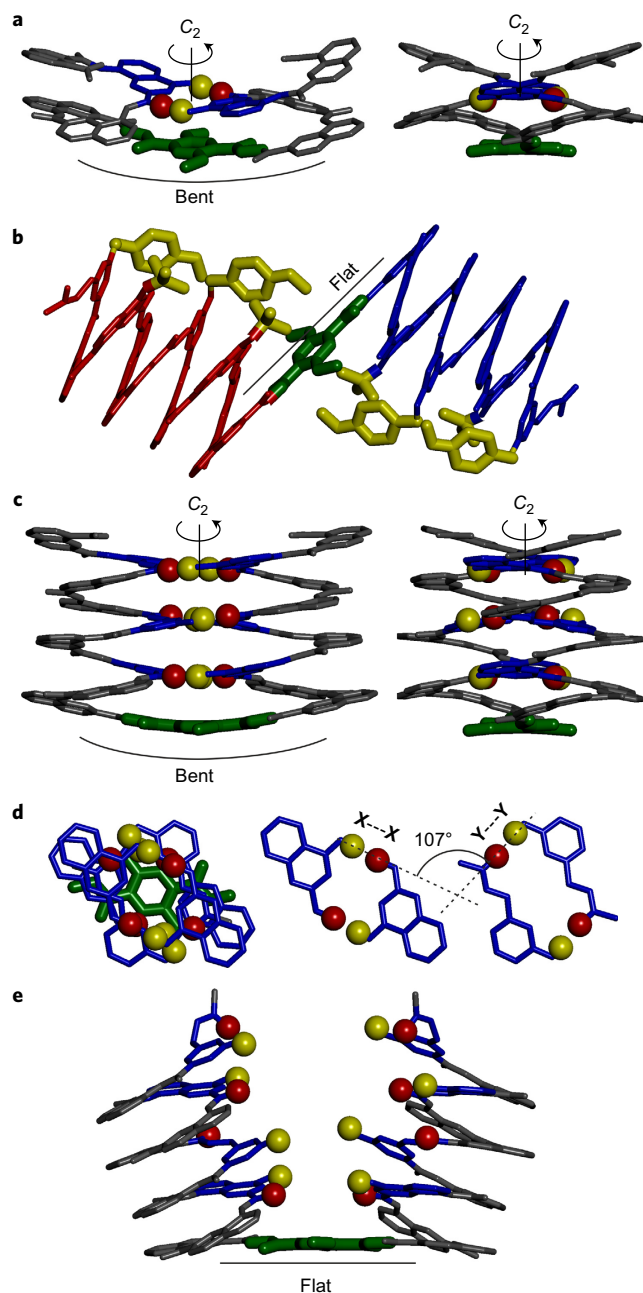


Figure 3 | Helix-turn-helix motifs in the solid state. a–e, Crystal structures of **1a** (a), **2b** (b), **3a** (c,d) and **2a** (e) represented at the same scale. A top view of the stack of X, Y and T units of the structure of **3a** is shown on the left of d. The central and right structures in d are hydrogen-bonded pairs of X units and of Y units, respectively, translated horizontally from the stack, and show a distinct orientation of the hydrogen bonds. The hydroxyl protons and carbonyl oxygen atoms of the hydrogen-bonding arrays are shown as yellow and red balls, respectively. X and Y units are shown as blue tubes, except in b, where blue tubes are for the P helix and red tubes for the M helix. In b, the PMB and ^tBu protecting groups are shown as thick yellow tubes. For clarity, the ^tBuO side chains of the Q units, included solvent molecules and most hydrogen atoms have been omitted, and only the oxygen atom and the first carbon of each ^tBuO chain of the T units are shown (in green).

CH groups responsible for steric hindrance⁴¹. Modelling predicts that this monomer may allow the formation of two additional inter-helix hydrogen bonds that involve the amide carbonyl of the next unit (Fig. 1d,i).

Sequence **2a** was then prepared. Its two helices each consists of two contiguous YQXQQ segments. Q_n sequences have been shown to span about five units per two turns⁴¹, which suggests that inter-helix hydrogen-bonds of consecutive pentads may be in register. This assumption is to be related to the behaviour of heptad repeat motifs of α -peptidic zippers¹⁹. Heptads would be in perfect register if the α -helix spanned 3.5 units per turn. The fact that curvature is closer to 3.6 units per turn forces some adjustments, that is, coil coiling, to maintain the helix-helix interactions over long distances¹⁹. Sequence **2a** contains one turn unit and 20 δ -amino acids, each of which has the same backbone length as a dipeptide. In terms of molecular weight, sequence **2a** is comparable to that of a 42mer peptide, which is larger than is required for small tertiary folds to form^{42–44}. The ¹H NMR spectrum of the protected sequence **2b** again shows two sets of signals, which reflects the coexistence of *PP/MM* and *PM* species (Fig. 2d). In this case, one species is strongly favoured and can be assigned to the *PM* conformer by the crystal structure and the NMR spectrum of freshly dissolved crystals (Fig. 3b and Supplementary Fig. 6). The crystal structure shows that four ⁴Bu and four PMB protecting groups would be in contact and generate hindrance if the helices were on the same side of the turn, that is, in the *PP/MM* conformer. On deprotection into **2a**, only one species is observed (Fig. 2e), which shows that the two helices interact so as to bias the equilibrium completely. Diffusion-ordered spectroscopy (DOSY) NMR spectra testified that **2a** is monomeric in solution: **2a** and **2b** have similar diffusion coefficients (Supplementary Figs 7 and 8). The assignment of OH protons to downfield-shifted resonances between 9 and 10 ppm indicates their involvement in hydrogen bonds (Supplementary Fig. 9). As our initial attempts to crystallize **2a** failed, sequence **3a** was prepared. Its helical segments are both one unit shorter than in **2a** and are terminated by nitroquinoline rings instead of acetylaminomethyl groups, a feature that we have observed to favour crystallization. The crystal structure of **3a** (Fig. 3c,d and Supplementary Movie 1) validated the predicted helix-turn-helix motif: no steric clash occurred and all six expected inter-helix hydrogen bonds were established (Fig. 1b,d), with the two helices maintained in a parallel orientation with the same handedness. In CDCl₃, **3a** shows spectral features similar to those of **2a** (one set of sharp signals), whereas its protected precursor **3b** shows two sets (Supplementary Fig. 10).

Eventually, diffracting crystals of **2a** were obtained from dimethylformamide. From this polar solvent, an open ('unfolded') *PP/MM* form crystallized (Fig. 3e). This observation triggered the investigation of the solvent dependence of the helix-turn-helix motif. No denaturation of **2a** was observed by NMR spectroscopy on heating in C₂D₂Cl₄ up to 70 °C, which reflects the high stability and hints at a small entropy of folding. However, the addition of hydrogen-bonding solvents disrupted the tertiary fold. No folding occurs in DMSO-*d*₆ (DMSO, dimethylsulfoxide) or pyridine-*d*₅, as judged by the presence of both *PP/MM* and *PM* species (Supplementary Fig. 11). Remarkably, DMSO-induced unfolding of **2a** occurs through a sharp transition between 18 and 23% (vol/vol) of the polar solvent (Fig. 2f and Supplementary Fig. 12), indicative of a cooperative phenomenon. Nothing similar was observed for **2b** (Supplementary Fig. 15), which confirms that the changes observed for **2a** reflect a conformational transition and not a solvent dependence of chemical shift values. A similar transition is observed for **1a**, but it is less sharp and requires less DMSO (Supplementary Figs 13 and 14). Changes in NMR spectra during the transitions support the existence of two equilibria shown in Fig. 2g. The first equilibrium (K_1) between the folded *PP* (or *MM*) helix-turn-helix and its unfolded form is solvent dependent and rapid on the NMR timescale—adding DMSO causes chemical shift variations as the proportions between the two species vary (Fig. 2f,g). The second equilibrium between unfolded *PP/MM* and *PM* conformations is slow on the NMR timescale. Unfolding thus

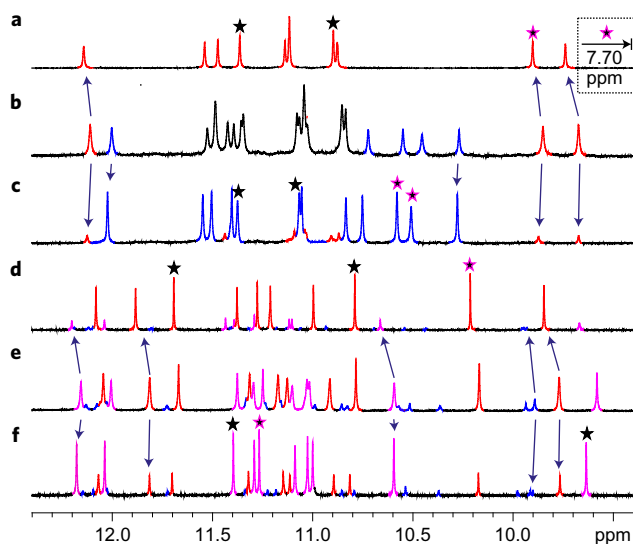


Figure 4 | Solution studies of helix bundles. **a–c**, Extracts of ¹H NMR spectra that show NH and OH resonances at 400 MHz of 3.0 mM solutions of **4a** in CDCl₃ (**a**), **4a** in CDCl₃/CD₂Cl₂ (1:1 vol/vol) (**b**) and **4a** in CD₂Cl₂ (**c**). **d–f**, Extracts of ¹H NMR spectra that show NH and OH resonances at 700 MHz of 1.5 mM solutions of **5a** in CDCl₃ (**d**), **5a** in CDCl₃/CD₂Cl₂ (1:1 vol/vol) (**e**) and **5a** in CD₂Cl₂ (**f**). Red and magenta lines are assigned to homochiral dimeric helix bundles with tilted axes; blue lines are assigned to parallel homochiral trimeric helix bundles. Black lines indicate overlapping signals of the various species. Black stars indicate X–OH signals; magenta stars indicate Y–OH. Some arrows denote the corresponding signals in the various solvents.

also goes along with the emergence of the signals of the *PM* conformer, whose protons resonate at frequencies that vary little with the proportion of DMSO (Supplementary Fig. 12). The sharp transition between the folded and unfolded state is related to the overall rigidity of the helix backbone, which makes it difficult to not establish all the inter-helix hydrogen bonds at the same time. Unfolding does not proceed progressively, but through the simultaneous disruption of all hydrogen bonds. In addition, the folded helix-turn-helix is somewhat spring loaded. X-ray structures of **1a** and **3a** show a certain level of bending of the turn units (Fig. 3a,c), whereas it is flat in the unfolded state (Fig. 3b,e). This bending had been predicted by modelling (Fig. 1g–i) and reflects that the turn is actually slightly longer than the inter-helix distance in the folded state. Furthermore, helix curvature in the helix-turn-helix is slightly reduced with respect to its conformation in a relaxed state (Supplementary Fig. 51), which suggests a certain level of strain that is compensated by hydrogen bonding.

Formation of quaternary structures. We then explored the capacity of inter-helix hydrogen bonds to act intermolecularly. In the absence of a turn unit, additional degrees of freedom are allowed. For instance, **T** imposes hydrogen bonding to occur in register between helices with the same handedness and parallel C→N sequence polarity. In the absence of **T**, out of register, antiparallel arrangements and association between *P* and *M* helices are allowed. The deca-amide sequence **4a** spans four helix turns and possesses two **X** and two **Y** units. Despite the possibilities mentioned above, its ¹H NMR spectrum in CDCl₃ shows one set of sharp lines (Fig. 4a). Three OH resonances are found at 9.90, 10.90 and 11.36 ppm, which indicates their involvement in hydrogen bonds, but the fourth is not ($\delta = 7.70$ ppm). A DOSY spectrum of a 1:1 mixture of **4a** and its protected form, **4b**, shows that **4a** is larger even though it has a lower molecular weight, which indicates an aggregated state (Supplementary Figs 18 and 19).

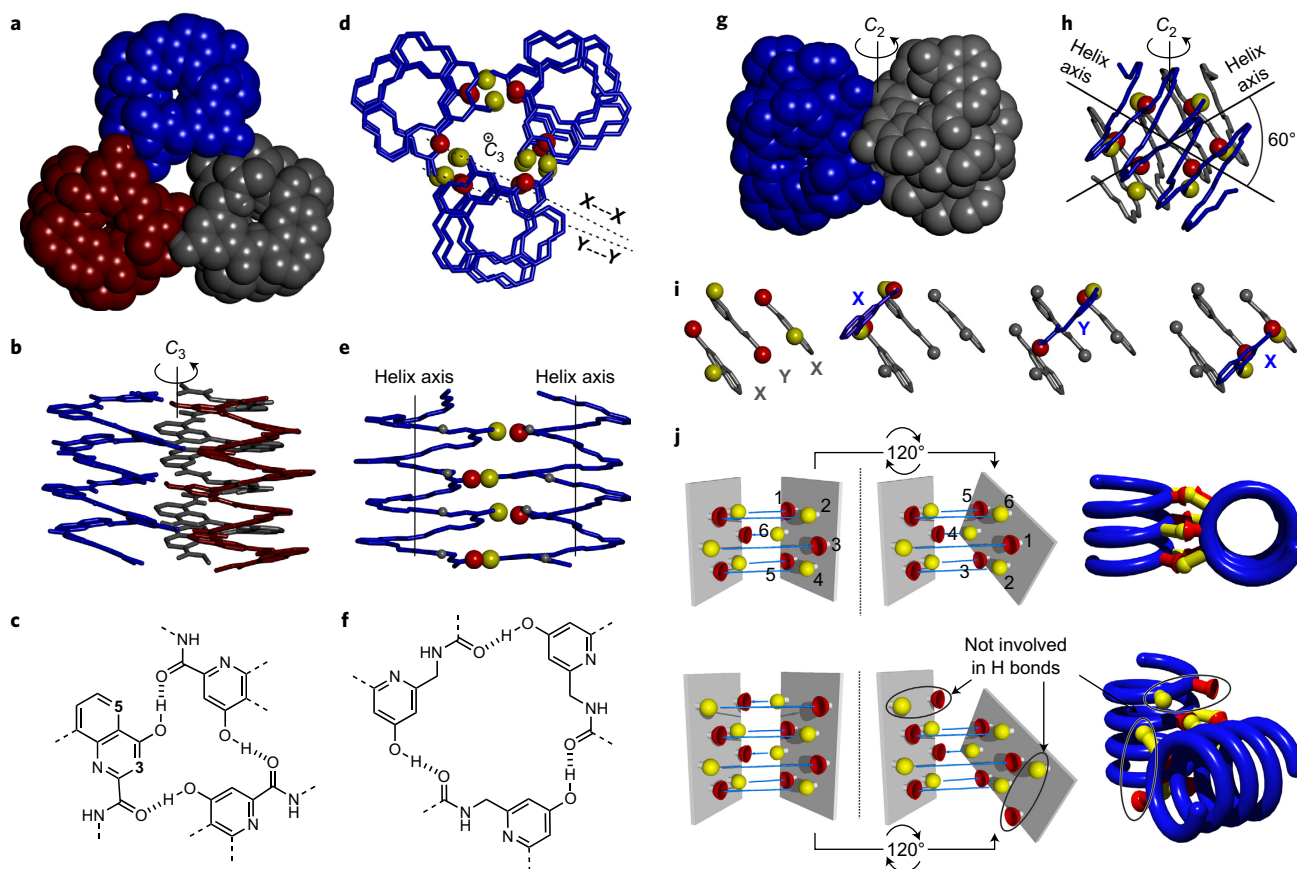


Figure 5 | Helix bundles in the solid state. **a–j**, Crystal structures of $(4a)_3$ (**a–f**) and $(5a)_2$ (**g–i**). In all representations, i BuO side chains of **Q** units, included solvent molecules and most hydrogen atoms have been omitted for clarity. **a,b**, Top view (CPK (Corey–Pauling–Koltun) representation) (**a**) and side view (tube) (**b**) of the trimeric helix bundle $(4a)_3$. **d,e**, Top view (**d**) and side view (**e**) of $(4a)_3$ that show hydrogen-bond donors and acceptors as golden yellow and red spheres, respectively. Only the outer rim of the helices is shown as a blue tube. In **e**, only two helices and one array of inter-helix hydrogen bonds are shown. **c,f**, Hydrogen-bonded trimeric arrangements of **X** and **Y** units. In **c**, OH groups point towards position 5 of the **X** unit to which they belong, in contrast with the helix–turn–helix structures in which the OH groups point towards position 3 (Fig. 1b). The dashed grey lines in **d** show that the $X \cdots X$ and $Y \cdots Y$ hydrogen bonds are almost parallel, in contrast with the structure of **3a** (Fig. 3d). **g**, Side view of the tilted dimeric bundle $(5a)_2$ (CPK representation). **h**, The front view of $(5a)_2$ shows the 60° tilt angle between the helix axes. Hydrogen-bond donors and acceptors are shown as yellow and red spheres, respectively. Only the outer rim of the helices is shown, as a blue tube. **i**, Same view as in **h**, but showing exclusively the **X** and **Y** units of one helix in grey (left) and each of the hydrogen-bonded **X** and **Y** units of the other helix in blue. **j**, Schematic representation of how a given array of six hydrogen-bond donors (yellow) and acceptors (red) may allow hydrogen bonding both in a parallel arrangement, and after a 120° rotation.

The aggregate does not dissociate on diluting down to 0.30 mM. On adding CD_2Cl_2 , a second set of signals emerges, which indicates the presence of a distinct structure that becomes major in pure CD_2Cl_2 (Fig. 4b,c). In this structure, all the OH groups are involved in hydrogen bonds ($\delta = 10.51, 10.58, 11.07$ and 11.37 ppm). The exchange between the two species is very slow, which shows that considerable rearrangements are needed for their interconversion. For instance, evaporating an equilibrated CD_2Cl_2 sample and dissolving the residue in $CDCl_3$ requires monitoring over 30 minutes (Supplementary Figs 24–30). This hints at an interconversion mechanism that involves the simultaneous disruption of all the hydrogen bonds within the aggregates, possibly via a disfavoured monomeric state.

A crystal structure of **4a** revealed the formation of a trimeric helix bundle that comprised three helices with the same handedness, parallel helix axes and identical C→N sequence polarity (Fig. 5a–f and Supplementary Movie 2). A total of 12 hydrogen bonds are established between the **X** units and between the **Y** units within $(4a)_3$, similar to the eight hydrogen bonds of helix–turn–helix **3a**. However, hydrogen-bond orientation is different: in both structures O \cdots H–O angles are all close to 180° , but C=O \cdots H angles are also close to 180° in **3a**, whereas they are closer to 120° in $(4a)_3$.

In $(4a)_3$, hydroxyl protons thus point straight to carbonyl lone pairs, an orientation that has been shown to be favoured⁴⁵, but that is made impossible in **2a** and **3a** because of restrictions imposed by turn units.

The NMR spectrum of freshly dissolved crystals of $(4a)_3$ shows that this is the dominant species in CD_2Cl_2 (Supplementary Fig. 23), consistent with the observation that all the OH groups are involved in hydrogen bonds (Fig. 4c). Dilution causes the dissociation of $(4a)_3$ into one other species, which, we have shown above, is also an aggregate, and therefore cannot be anything other than dimeric (Supplementary Fig. 32). Ion mobility mass spectrometry (IMS) measurements confirm the coexistence of dimeric and trimeric aggregates (Supplementary Fig. 21). The concentration dependence allows us to quantify the equilibrium between dimers ($2x$) and trimers ($3x$): $3x(4a)_2 \rightleftharpoons 2x(4a)_3$ (K_{4a}) with $K_{4a} = 2.2 \times 10^5 M^{-1}$ in CD_2Cl_2 and $<0.2 M^{-1}$ in $CDCl_3$. We also found that other solvents (CCl_4 , $C_2D_2Cl_4$ and toluene) affect this equilibrium in various ways (Supplementary Fig. 33). The reason for this solvent dependence is unclear. Pyridine and DMSO cause the dissociation of all aggregates into monomeric helices (Supplementary Fig. 34). The effect is more progressive and less cooperative than in the helix–turn–helix bundle.

The solution behaviour of the shorter sequence **5a** shed light on the nature of (**4a**)₂. Its ¹H NMR spectrum in CDCl₃ shows a major species and two distinct minor species (Fig. 4d). A DOSY spectrum of a mixture of **4b** and **5a** in CDCl₃ indicates a larger size for the latter, which must therefore be a well-defined aggregate (Supplementary Figs 16 and 17). On adding CD₂Cl₂, the proportion of one of the two other species increased to become major in pure CD₂Cl₂, whereas the third species remained minor (Fig. 4e,f). In both major species, all the OH groups are hydrogen bonded. Their relative proportion does not depend on the concentration, which indicates that they are composed of the same number of molecules. In contrast, the proportion of the minor species increases with increasing concentration, which shows that it has a higher molecularity (Supplementary Fig. 31). Dissolving crystals of **5a** (see below) allowed us to assign the two dominant species to dimers (**5a**)₂. IMS also registered the presence of a trimeric aggregate (Supplementary Fig. 20). The minor NMR signals were thus assigned to a trimer, (**5a**)₃, which may be similar to (**4a**)₃. The equilibrium constant between the two dimers, $\text{dimer}_{\text{CDCl}_3} \rightleftharpoons \text{dimer}_{\text{CD}_2\text{Cl}_2}$, was calculated to be $K_{5a} = 2.5$ in CD₂Cl₂ and 0.24 in CDCl₃. Again, we found no obvious explanation for the solvent dependence.

The structure in the solid state of the species that prevails in CD₂Cl₂ was elucidated (Fig. 5g–i and Supplementary Movie 3), its identity being established by NMR spectra of freshly dissolved crystals (Supplementary Fig. 22). It shows a dimeric arrangement of two helices with the same handedness. The two helix axes are not parallel, but tilted by 120° anticlockwise (for *P* helices) with respect to the expected parallel head-to-head arrangement (or 60° clockwise with respect to a parallel head-to-tail arrangement (Fig. 5h)). All the hydroxyl groups are involved in hydrogen bonds, but these are not established between homomeric pairs of *X* or *Y* units, but directly between *X* and *Y* (Fig. 5i). As depicted in Fig. 5j (top), the positions of hydrogen-bonding sites in one face of a helix can be rotated by 120° and still lead to a matching array of donors and acceptors. The consequence of the 120° tilt in a helix having not six but eight hydrogen bonding sites, as in **4a**, is that two hydrogen-bonding sites will be unoccupied (Fig. 5j, bottom). This is consistent with the ¹H NMR spectrum of (**4a**)₂ in CDCl₃, which can reasonably be assigned to a tilted dimer apparently favoured in this solvent.

The nature of the (**5a**)₂ dimer that prevails in CDCl₃ can be proposed based on the partial assignment of NMR spectra and remarkable nuclear Overhauser effect (NOE) correlations within the various complexes of **4a** and **5a** (Supplementary Figs 35–46). Head-to-head arrangements of the helices of opposite handedness can be ruled out because they lead to *X*–*X* and *Y*–*Y* mismatches (donors facing donors, acceptors facing acceptors), or *X*–*Y* mismatches (different distances between pairs of donors and acceptors). The parallel head-to-head arrangement of helices of identical handedness, as found in the structure of **3a**, are less favoured, as the formation of (**4a**)₃ demonstrates. A similar head-to-tail arrangement of helices of opposite handedness (Supplementary Fig. 47) is also ruled out based on the observed NOEs. Tilted arrangements of helices of opposite handedness (Supplementary Fig. 48) can also be ruled out because they would have no symmetry element and give rise to twice the number of ¹H resonances actually observed (that is, no degeneracy). Finally, the only remaining and most-probable option is that the (**5a**)₂ dimer that prevails in CDCl₃ is also a tilted dimer between helices of identical handedness, thus like (**4a**)₂ in this solvent, but with a tilt direction opposite to that shown in Fig. 5h (Supplementary Figs 47–50).

Conclusion

Using simple computational considerations, hydrogen bonding has been designed at defined locations on aromatic amide backbones that eventually promotes cooperative folding into helix–turn–helix

motifs in organic solvents. This approach rested on the inherent stability of aromatic amide helices and may be extended to interacting functionalities other than aromatic hydroxyl and amide carbonyl groups. The hydrogen-bond-directed aggregation of helices not linked by a turn unit produced several thermodynamically and kinetically stable dimeric and trimeric homochiral bundles with structures distinct from the designed helix–turn–helix. The relative helix orientation within the bundles may be changed from parallel to tilted on subtle solvent variations, such as replacing dichloromethane by chloroform. Altogether, these results prefigure the richness and uniqueness of abiotic tertiary-structure behaviour. To combine parallel and tilted motifs in the same structure using appropriately designed turn units would yield yet another level of complexity in abiotic tertiary folding. The high stability and rigidity of the helix bundles presented here allow us to speculate that they might accommodate the presence of more-flexible backbone features. This would, in turn, enhance folding entropy and result in melting of the structures on heating in a tunable fashion. Progress along these lines is being made and will be reported in due course.

Data availability. Crystallographic data for **1a**, **2a**, **2b**, **3a**, **4a** and **5a** have been deposited with the Cambridge Crystallographic Data Centre under reference numbers CCDC-1450791, 1451415, 1469843, 1451523, 1470116 and 1451494, respectively. These data can be obtained free of charge from the Cambridge Crystallographic Data Centre (http://www.ccdc.cam.ac.uk/data_request/cif). Other data that support the findings of this study (spectroscopic or mass spectrometric data) are available from the corresponding author on reasonable request.

Received 16 January 2017; accepted 27 July 2017;
published online 18 September 2017

References

- Guichard, G. & Huc, I. Synthetic foldamers. *Chem. Commun.* **47**, 5933–5941 (2011).
- Zhang, D. W., Zhao, X., Hou, J. L. & Li, Z. T. Aromatic amide foldamers: structures, properties, and functions. *Chem. Rev.* **112**, 5271–5316 (2012).
- Gellman, S. H. Foldamers: a manifesto. *Acc. Chem. Res.* **31**, 173–180 (1998).
- Goodman, C. M., Choi, S., Shandler, S. & DeGrado, W. F. Foldamers as versatile frameworks for the design and evolution of function. *Nat. Chem. Biol.* **3**, 252–262 (2007).
- Nair, R. V., Vijayadas, K. N., Roy, A. & Sanjayan, G. J. Heterogeneous foldamers from aliphatic-aromatic amino acid building blocks: current trends and future prospects. *Eur. J. Org. Chem.* **2014**, 7763–7780 (2014).
- Lokey, R. S. & Iverson, L. B. Synthetic molecules that fold into a pleated secondary structure in solution. *Nature* **375**, 303–305 (1995).
- Brüggemann, J. *et al.* Spontaneous knotting—from oligoamide threads to trefoil knots. *Angew. Chem. Int. Ed.* **46**, 254–259 (2007).
- Ponnuwamy, N., Coughon, F. B. L., Clough, J. M., Pantoş, G. D. & Sanders, J. K. M. Discovery of an organic trefoil knot. *Science* **338**, 783–785 (2012).
- Hua, Y., Liu, Y., Chen, C. H. & Flood, A. H. Hydrophobic collapse of foldamer capsules drives picomolar-level chloride binding in aqueous acetonitrile solutions. *J. Am. Chem. Soc.* **135**, 14401–14412 (2013).
- Chandramouli, N. *et al.* Iterative design of a helically folded aromatic oligoamide sequence for the selective encapsulation of fructose. *Nat. Chem.* **7**, 334–341 (2015).
- Huang, P.-S. *et al.* *De novo* design of a four-fold symmetric TIM-barrel protein with atomic-level accuracy. *Nat. Chem. Biol.* **12**, 29–34 (2016).
- Boyken, S. E. *et al.* *De novo* design of protein homo-oligomers with modular hydrogen-bond network-mediated specificity. *Science* **352**, 680–687 (2016).
- Hilvert, D. Design of protein catalysts. *Annu. Rev. Biochem.* **82**, 447–470 (2013).
- Khoury, G. A., Smadbeck, J., Kieslich, C. A. & Floudas, C. A. Protein folding and *de novo* protein design for biotechnological applications. *Trends Biotechnol.* **32**, 99–109 (2014).
- Parmeggiani, F. *et al.* A general computational approach for repeat protein design. *J. Mol. Biol.* **427**, 563–575 (2015).
- Price, J. L. *et al.* Design of a three-helix bundle capable of binding heavy metals in a triscysteine environment. *Angew. Chem. Int. Ed.* **49**, 368–371 (2010).
- Grigoryan, G. & DeGrado, W. F. Probing designability via a generalized model of helical bundle geometry. *J. Mol. Biol.* **405**, 1079–1100 (2011).
- Joh, N. H. *et al.* *De novo* design of a transmembrane Zn²⁺-transporting four-helix bundle. *Science* **346**, 1520–1524 (2014).

19. Woolfson, D. N. The design of coiled-coil structures and assemblies. *Adv. Protein Chem.* **70**, 79–112 (2005).
20. Gradišar, H. *et al.* Design of a single-chain polypeptide tetrahedron assembled from coiled-coil segments. *Nat. Chem. Biol.* **9**, 362–366 (2013).
21. Reinert, Z. E., Lengyel, G. A. & Horne, W. S. Protein-like tertiary folding behavior from heterogeneous backbones. *J. Am. Chem. Soc.* **135**, 12528–12531 (2013).
22. Mayer, C., Müller, M. M., Gellman, S. H. & Hilvert, D. Building proficient enzymes with foldamer prostheses. *Angew. Chem. Int. Ed.* **53**, 6978–6981 (2014).
23. Tavenor, N. A., Reinert, Z. E., Lengyel, G. A., Griffith, B. D. & Horne, W. S. Comparison of design strategies for α -helix backbone modification in a protein tertiary fold. *Chem. Commun.* **52**, 3789–3792 (2016).
24. Horne, W. S., Price, J. L., Keck, J. L. & Gellman, S. H. Helix-bundle quaternary structure from α/β -peptide foldamers. *J. Am. Chem. Soc.* **129**, 4178–4180 (2007).
25. Cheng, P. N., Pham, J. D. & Nowick, J. S. The supramolecular chemistry of β -sheets. *J. Am. Chem. Soc.* **135**, 5477–5492 (2013).
26. Kreutzer, A. G., Hamza, I. L., Spencer, R. K. & Nowick, J. S. X-ray crystallographic structures of a trimer, dodecamer, and annular pore formed by an $A\beta_{17-36}$ β -hairpin. *J. Am. Chem. Soc.* **138**, 4634–4642 (2016).
27. Daniels, D. S., Petersson, E. J., Qiu, J. X. & Schepartz, A. High-resolution structure of a β -peptide bundle. *J. Am. Chem. Soc.* **129**, 1532–1533 (2007).
28. Petersson, E. J., Craig, C. J., Daniels, D. S., Qiu, J. X. & Schepartz, A. Biophysical characterization of a β -peptide bundle: comparison to natural proteins. *J. Am. Chem. Soc.* **129**, 5344–5345 (2007).
29. Collie, G. W. *et al.* Shaping quaternary assemblies of water-soluble non-peptide helical foldamers by sequence manipulation. *Nat. Chem.* **7**, 871–878 (2015).
30. Sharma, G. V. M. *et al.* Design and synthesis of peptides with hybrid helix–turn–helix (HTH) motif and their conformational study. *J. Org. Chem.* **79**, 8614–8628 (2014).
31. Delsuc, N., Massip, S., Léger, J. M., Kauffmann, B. & Huc, I. Relative helix–helix conformations in branched aromatic oligoamide foldamers. *J. Am. Chem. Soc.* **133**, 3165–3172 (2011).
32. Ichinose, W., Ito, J. & Yamaguchi, M. Tetrameric $\alpha\alpha\beta\beta$ aggregate formation by stereoisomeric bidomain helicene oligomers. *Angew. Chem. Int. Ed.* **52**, 5290–5294 (2013).
33. Gan, Q. *et al.* Translation of rod-like template sequences into homochiral assemblies of stacked helical oligomers. *Nat. Nanotech.* **12**, 447–452 (2017).
34. Kent, S. B. H. Total synthesis of proteins. *Chem. Soc. Rev.* **38**, 338–351 (2009).
35. Pusterla, I. & Bode, J. W. An oxazetidine amino acid for chemical protein synthesis by rapid, serine-forming ligations. *Nat. Chem.* **7**, 668–672 (2015).
36. Haj-Yahya, M. *et al.* Synthetic polyubiquitinated α -synuclein reveals important insights into the roles of the ubiquitin chain in regulating its pathophysiology. *Proc. Natl Acad. Sci. USA* **110**, 17726–17731 (2013).
37. Jiang, H., Léger, J. M. & Huc, I. Aromatic δ -peptides. *J. Am. Chem. Soc.* **125**, 3448–3449 (2003).
38. Delsuc, N. *et al.* Kinetics of helix-handedness inversion: folding and unfolding in aromatic amide oligomers. *ChemPhysChem* **9**, 1882–1890 (2008).
39. Qi, T. *et al.* Solvent dependence of helix stability in aromatic oligoamide foldamers. *Chem. Commun.* **48**, 6337–6339 (2012).
40. Maurizot, V. *et al.* Design of an inversion center between two helical segments. *J. Am. Chem. Soc.* **126**, 10049–10052 (2004).
41. Sánchez-García, D. *et al.* Nanosized hybrid oligoamide foldamers: aromatic templates for the folding of multiple aliphatic units. *J. Am. Chem. Soc.* **131**, 8642–8648 (2009).
42. Neidigh, J. W., Fesinmeyer, R. M. & Andersen, N. H. Designing a 20-residue protein. *Nat. Struct. Biol.* **9**, 425–430 (2002).
43. Hodges, A. M. & Schepartz, A. Engineering a monomeric miniature protein. *J. Am. Chem. Soc.* **129**, 11024–11025 (2007).
44. Craven, T. W., Cho, M. K., Traaseth, N. J., Bonneau, R. & Kirshenbaum, K. A miniature protein stabilized by a cation– π interaction network. *J. Am. Chem. Soc.* **138**, 1543–1550 (2016).
45. Lommerse, J. O. S. P. M., Price, S. L. & Taylor, R. Hydrogen bonding of carbonyl, ether, and ester oxygen atoms with alkanol hydroxyl groups. *J. Comput. Chem.* **18**, 757–774 (1997).

Acknowledgements

This work was supported by the European Research Council under the European Union's Seventh Framework Programme (Grant Agreement no. ERC-2012-AdG-320892), by the European Union under the People program (FP7 PIIF-2009-254156 postdoctoral fellowship to T.Q.) and by the French–Chinese Foundation for Science and its Applications (postdoctoral fellowship to B.C.). The contribution of S. Post in optimizing the synthesis of 4'-BuO-protected quinoline monomers is acknowledged. The authors thank B. Kauffmann for assistance with X-ray data collection and structure resolution at the Institut Européen de Chimie et Biologie's X-ray diffraction facility and M. Ferrer for beam time and help during the data collection on FIP-BM30A at the European Synchrotron Radiation Facility.

Author contributions

S.D. and B.C. contributed equally to this work. S.D., B.C. and T.Q. synthesized all the new compounds, carried out the solution studies and grew single crystals. T.G. refined the crystal structures. I.H. and V.M. designed the research and carried out the modelling studies. I.H. wrote the manuscript. All the authors discussed the results and commented on the manuscript.

Additional information

Supplementary information is available in the [online version of the paper](#). Reprints and permissions information is available online at www.nature.com/reprints. Publisher's note: Springer Nature remains neutral with regard to jurisdictional claims in published maps and institutional affiliations. Correspondence and requests for materials should be addressed to I.H.

Competing financial interests

The authors declare no competing financial interests.